

# QM/MM Studies of Xanthine Oxidase: Variations of Cofactor, Substrate, and Active-Site Glu802

Sebastian Metz and Walter Thiel\*

Max-Planck-Institut für Kohlenforschung, D-45470 Mülheim an der Ruhr, Germany

Received: October 19, 2009

In continuation of our previous QM/MM study on the reductive half-reaction of wild-type xanthine oxidase, we consider the effects of variations in the cofactor, the substrate, and the active-site Glu802 residue on the reaction mechanism. Replacement of the sulfido ligand in the natural cofactor by an oxo ligand leads to a substantial increase in the computed barriers, consistent with the experimentally observed inactivity of this modified cofactor, whereas the selenido form is predicted to have lower barriers and hence higher activity. For the substrate 2-oxo-6-methylpurine, the calculated pathways for three different tautomers show great similarity to those found previously for xanthine, contrary to claims in the literature that the mechanisms for these two substrates are different. Compared with the wild-type enzyme, the conversion of xanthine to uric acid follows a somewhat different pathway in the Glu802 → Gln mutant which exhibits a lower overall activity, in agreement with recently published kinetic data. The present results confirm the basic stepwise reaction mechanism and the orientation of the substrate that has been proposed in our previous QM/MM work on aldehyde oxidoreductase and xanthine oxidase.

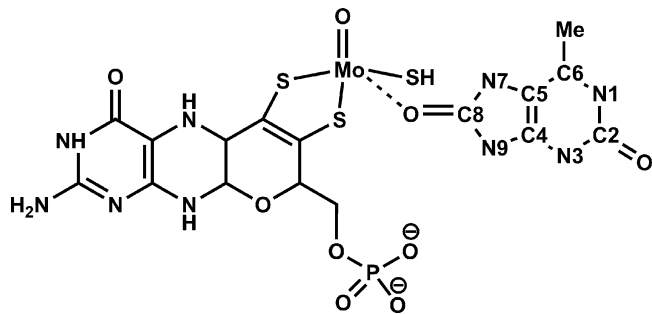
## 1. Introduction

The conversion of xanthine to uric acid is catalyzed by two molybdopterin containing enzymes, xanthine oxidase (XO, giving the name to the whole structural family<sup>1</sup>) and xanthine dehydrogenase (XDH). These enzymes have been studied for more than 100 years.<sup>2,3</sup> Contrary to many other oxygenases, they use water instead of elementary O<sub>2</sub> as their ultimate oxygen source<sup>4</sup> and they generate two reductive equivalents rather than consuming them.

Mechanistic information on the reductive half-reaction for the xanthine oxidase family was inferred from docking studies of xanthine in the structurally similar aldehyde oxidoreductase (AOR),<sup>5,6</sup> from the crystal structures of XO and XDH,<sup>7–9</sup> and from kinetic experiments with xanthine and other substrates of XO.<sup>10–13</sup> A Lewis-base-catalyzed mechanism involving the active-site glutamate residue (Glu1261 in XO and Glu869 in AOR) was proposed on the basis of these data.<sup>6–9,11,12</sup> Recent quantum mechanical/molecular mechanical (QM/MM) calculations<sup>14,15</sup> confirmed the general features of this mechanism and provided detailed insight into several competing pathways and the nature of the postulated intermediates.<sup>16</sup>

Substrate orientation within the enzyme was controversial for a long time. An “upside” conformation of xanthine relative to the molybdopterin cofactor was found in early modeling studies in 1996<sup>6</sup> and widely accepted thereafter. For the inactive oxo form of XO, this orientation of xanthine was recently proven by X-ray crystallography.<sup>17</sup> On the other hand, allopurinol<sup>18</sup> and 2-oxo-6-methylpurine,<sup>9</sup> both substrates similar to xanthine, are oriented “upside down” in their crystal structures (see Scheme 1). Therefore, different orientations for “good” substrates such as xanthine and “poor” substrates such as 2-oxo-6-methylpurine were postulated to explain the different reactivities.<sup>8,9</sup> By contrast, Yamaguchi et al.<sup>12</sup> proposed a reaction mechanism in which xanthine adopts the same “upside down” orientation as

**SCHEME 1:** Reduced Molybdopterin Cofactor with Coordinated Product in the “Upside Down” Orientation, with the Numbering Scheme for the Nitrogen and Carbon Atoms in the Product



found for 2-oxo-6-methylpurine in the crystal structure. The QM/MM results<sup>15</sup> suggest that the “upside” conformation represents the thermodynamic minimum, whereas xanthine is oriented “upside down” in the kinetically active pathway.

Our recent QM/MM work addressed the reaction mechanism in XO<sup>15</sup> and in the similar AOR system.<sup>14</sup> There are several other theoretical investigations on model systems, dealing with formaldehyde,<sup>19–21</sup> formamide,<sup>21–24</sup> as well as imidazole, xanthine, and several methylxanthines<sup>25</sup> as substrates. Since these have been summarized before, we shall not review them again here, except for noting that most of these studies only deal with a concerted one-step mechanism, which is less favorable than a stepwise mechanism in the enzymatic environment.<sup>14,15</sup> In this work, we will focus on this stepwise mechanism for the conversion of xanthine to uric acid in XO and explore the question whether it remains valid in variants of this reaction, i.e., upon changes in the cofactor, the substrate, and the Glu802 residue. Motivated by the need to understand recent experimental data (see below), we will concentrate on the following three issues.

\* To whom correspondence should be addressed. E-mail: thiell@mpi-muelheim.mpg.de.

**Cofactor.** The catalytic activity of XO is lost when the sulfido ligand in the cofactor is replaced by an oxo ligand.<sup>26</sup> We will study the reaction of xanthine in XO with the cofactor in its oxo form and also monitor the influence of a selenido ligand which is present in the nicotinate dehydrogenase system.<sup>27</sup> The lack of activity in the oxo form has been attributed to orbital effects in theoretical investigations of small model compounds.<sup>27</sup> We will provide a more detailed analysis, since we calculate the complete reaction pathway with all individual elementary steps and intermediates.

**Substrate.** The formation and decay of ESR active species following the reductive half-cycle of XO with xanthine as a substrate is rather fast. Therefore, 2-oxo-6-methylpurine was often used as a slower substrate to investigate this reaction experimentally.<sup>10,11,13,28,29</sup> However, it is not the conversion of the coordinated substrate to the product complex but the product release that makes 2-oxo-6-methylpurine a “slow” substrate.<sup>13</sup> Nevertheless, its lower overall reactivity led to the suggestion that xanthine and 2-oxo-6-methylpurine adopt different orientations within the binding pocket.<sup>8,17</sup> We will therefore study the reaction pathways of 2-oxo-6-methylpurine and compare them with those computed previously for xanthine in XO.

**Glu802.** Mutagenesis of active-site residues is a helpful tool to analyze their individual influence on the reactivity. Mutation of Glu1261 leads to a complete loss of activity<sup>30</sup> because it shuts down the initial proton transfer that is essential for the activation of the cofactor in XO. Arg880 influences both substrate binding and reaction rate,<sup>8,12</sup> by tuning the amount of electrostatic stabilization provided to the various forms of the substrate during the reaction.<sup>15</sup> Glu802 affects the reactivity of xanthine in XO only to a minor extent but plays a more pronounced role for hypoxanthine.<sup>12,30,31</sup> Recent experimental work with xanthine as a substrate has shown that the conservative mutation Glu802 → Gln in XO hardly changes the Michaelis constant ( $K_m$ (xanthine) =  $64.4 \pm 0.9 \mu\text{M}$  for the wild-type enzyme vs  $K_m$ (xanthine) =  $55.21 \pm 3.1 \mu\text{M}$  for the mutant), whereas the effective rate constant drops from  $k_{\text{cat}} = 108 \pm 1.5 \text{ s}^{-1}$  for the wild-type enzyme to  $1.16 \pm 0.08 \text{ s}^{-1}$  for the mutant.<sup>31</sup> We will analyze this change in reactivity due to the mutation of this “spectator residue” and demonstrate its impact on the mechanism.

This paper is organized as follows: In the next section, we describe the applied computational methods. In the following main section, we present and discuss the QM/MM results for the three topics outlined above. We conclude with a brief summary in the final section.

## 2. Computational Methods

**2.1. System Preparation and Classical Simulations.** To generate starting structures for the oxo and selenido forms of the cofactor and for the Glu802 → Gln mutant, we manually made the corresponding changes in the optimized structures from our previous study<sup>15</sup> and reoptimized them. For 2-oxo-6-methylpurine, we started from the previous solvated setup before the final 500 ps MD run,<sup>15</sup> manually replaced the substrate, and then performed a QM/MM optimization (with the QM region containing part of the cofactor, Glu1261, and the substrate). The resulting starting structures were relaxed by classical 15 ps MD simulations with some constraints: We defined an active region including all residues within 20 Å of the C8 atom of the substrate bound to the molybdopterin cofactor of chain A. Within this region, we kept the  $[\text{Mo}(\text{S}_2\text{C}_2\text{H}_2)(=\text{O})(\text{OR}_{\text{unfixed}})(-\text{SH})]^2-$  moiety and the  $\text{Fe}_2\text{S}_2$  cluster fixed during these simulations, while on the outside part of the water sphere (35 Å around the substrate C8 atom) we imposed a spherical

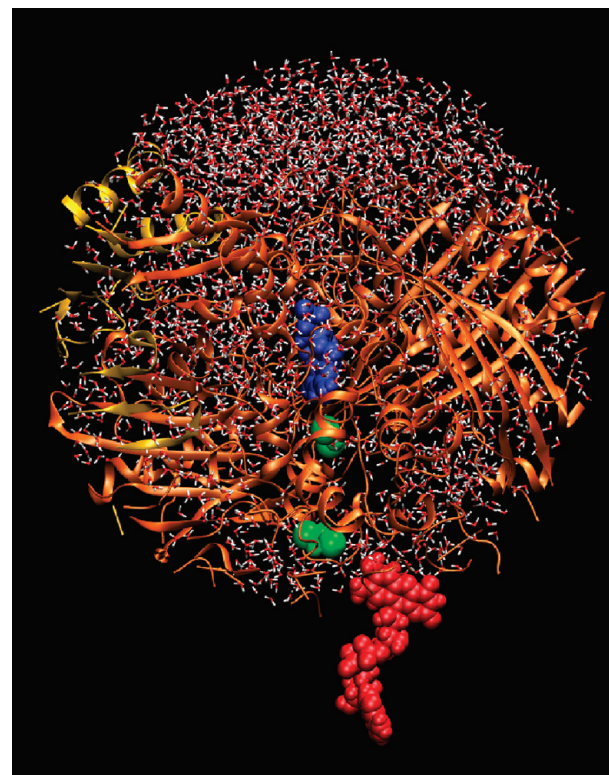


**Figure 1.** System used in the QM/MM calculations.

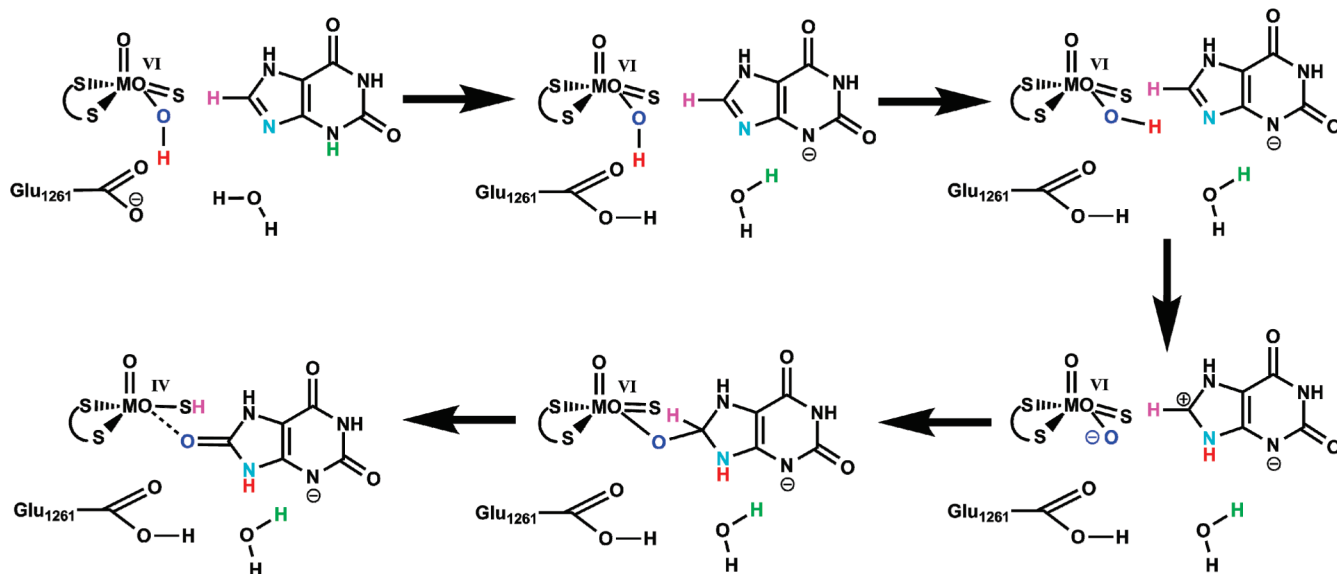
potential to prevent water molecules from escaping into the vacuum. A final 500 ps MD simulation at a temperature of 300 K using the CHARMM force field<sup>32</sup> as implemented in the CHARMM program package,<sup>33</sup> without imposing additional restraints, concluded the preparation of the enzyme–substrate complex.

As commonly accepted<sup>6–9,11,12</sup> and in analogy to our previous QM/MM work on XO<sup>15</sup> and AOR,<sup>14</sup> the substrate and Glu802 (Gln802) were neutral, Arg880 was protonated, and Glu1261 was deprotonated in all calculations. We adopted the same MM parameters as in our previous work<sup>14,15,34</sup> for the substrate, the molybdopterin cofactor, and the  $\text{Fe}_2\text{S}_2$  cluster. All nonstandard parameters are documented in the Supporting Information.

**2.2. QM/MM Setup.** We used the same neutral QM/MM system as in our previous XO study<sup>15</sup> (see Figure 1). QM/MM geometry optimizations of the stationary points were performed with a linear scaling microiterative algorithm working in hybrid delocalized coordinates.<sup>35</sup> All residues and water molecules within 13 Å of the substrate were included in the optimization; the remaining atoms were kept fixed. All QM/MM calculations were done with the modular program package ChemShell,<sup>36</sup> using TURBOMOLE<sup>37</sup> to obtain the QM(DFT) wave functions as well as the corresponding energies and gradients. MM energies and gradients were evaluated by DL\_POLY,<sup>38</sup> which is provided by the ChemShell package, using the CHARMM topology and parameter data. We used electrostatic embedding for the QM region.<sup>39</sup> No cutoff was applied on the rigid MM point charges, neither to calculate the electrostatic interaction within the MM region nor to calculate the electrostatic QM/MM interaction. To prevent overpolarization at the QM/MM boundary, we applied the charge-shift scheme.<sup>40,41</sup>

Different QM regions were employed in the QM/MM calculations which will be defined below on a case-by-case basis. The largest QM region included part of the cofactor, the substrate, and parts of the side chains of the Gln767, Glu802, Arg880, and Glu1261 residues and was used to perform

**SCHEME 2: Favored Mechanism for the Reaction of Xanthine within XO as Obtained in Our Previous QM/MM Study<sup>15</sup>**



COSMO<sup>42</sup> corrected single-point calculations to establish a common energy scale for the different setups.

Optimizations were generally first done using the BP86<sup>43–47</sup> functional with the resolution-of-the identity (RI) approximation<sup>48,49</sup> and then refined using the B3LYP hybrid functional<sup>43–45,50–52</sup> as implemented in TURBOMOLE. In the case of 2-oxo-6-methylpurine, we started from the product-bound structure and first determined the various minima along the reaction path. Easily detectable transition structures were localized starting from a preoptimized structure obtained by constrained minimization. In difficult cases, the nudged elastic band method<sup>53</sup> as implemented in DL-Find<sup>54</sup> was applied in combination with transition state optimization to find the minimum energy pathway as well as the transition state. The QM model calculations were performed using Gaussian 03.<sup>55</sup> All figures showing molecular structures were generated using VMD.<sup>56</sup>

Molybdenum was described by the Lanl2DZ basis set<sup>57</sup> augmented by an f polarization function,<sup>58</sup> sulfur and selenium by Lanl2DZ<sup>59</sup> with an additional d polarization function,<sup>60</sup> and all other atoms (C, H, N, O) by the 6-31+G\*\* basis set.<sup>61,62</sup> The RI-BP86 calculations employed the def2-TZV(P) auxiliary basis set.<sup>63</sup> This combination has already proven to give reasonable results.<sup>14,15,21</sup>

### 3. Results and Discussion

In a previous QM/MM study,<sup>15</sup> we investigated the conversion of xanthine to uric acid in XO using seven different setups that covered different tautomers and different orientations of xanthine as well as different protonation states of active-site residues. For the kinetically active “upside down” orientation (setup G),<sup>15</sup> the reaction starts with Glu1261 deprotonating xanthine at the N3 position followed by a proton transfer from the cofactor to the N9 atom of xanthine. The thus activated cofactor and substrate then react to form a tetrahedral intermediate, and a subsequent rate-limiting hydride transfer generates the product. The intermediates of this mechanism are sketched in Scheme 2, while the complete pathway is given in the Supporting Information (Figure S1). This most favorable pathway for xanthine in the wild-type enzyme (setup G) will serve as a reference mechanism in the present study of variants of the

previously studied system. In addition, we shall also consider a closely related pathway (setup F) and one conformation with the opposite “upside” orientation of the substrate (setup A) which was previously found to represent the thermodynamically most stable reactant complex.<sup>15</sup>

**3.1. Influence of the Hydride Acceptor in the Cofactor.** We modified the cofactor in XO and reoptimized the stationary points of the most favorable setup G (SN400) from our previous study to analyze the origin of the experimentally observed deactivation of XO upon replacement of the sulfido ligand by an oxo ligand<sup>26</sup> and to monitor the influence of a selenido ligand, that is present in the related nicotinate dehydrogenase.<sup>27</sup> We used the same QM region as before; see Figure 2. It is obvious from Table 1 that there is hardly any effect of the changed hydride acceptor on the relative energies of the various stationary points and the computed barriers, except for the hydride transfer reaction IM2 → TS3 → product, which shows a dramatically increased barrier for the oxido ligand and a slightly lower barrier when sulfur is replaced by selenium.

The lowering of the barrier for Se has been attributed to the smaller HOMO–LUMO gap between the Mo=Se  $\pi$  and  $\pi^*$  orbitals which should facilitate the rate-limiting hydride transfer step.<sup>27</sup> Indeed, we calculate the HOMO–LUMO gap to decrease from 2.35 eV (O) to 2.02 eV (S) and 1.95 eV (Se) in the intermediate IM2. We note, however, that the computed orbitals are quite delocalized in all relevant stationary points (IM2, TS3, product). Hence, there is no clear-cut  $\pi$  or  $\pi^*$  character, and neither the HOMO nor the LUMO orbital have significant electron density at the transferred H-atom (see Figure S2 in the Supporting Information).

An alternative explanation for the enhanced reactivity when going from the oxo to the sulfido and selenido form of the cofactor can be based on geometrical and energetic arguments. It is obvious that larger structural distortions of IM2 are needed to reach TS3 in the case of the oxo form (see Figure 2). For example, elongating the strong Mo=O bond by 0.13 Å is expected to cost more energy than stretching the weaker Mo=S and Mo=Se bonds by about 0.10 Å. Similar remarks apply to the changes in the Y–H and C–H distances. Looking from the product side, the H–Y bonds are longer by about 0.2 Å in TS3 which is again more difficult to achieve for H–O than for

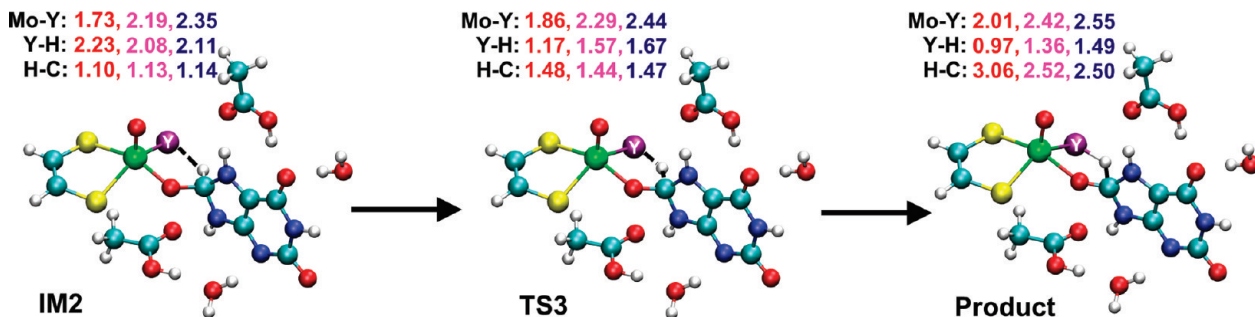


**Figure 2.** Hydride transfer step with key distances ( $\text{\AA}$ ) at the B3LYP/B1 level, for different forms of the cofactor:  $\text{Y} = \text{O}$  (red),  $\text{Y} = \text{S}$  (pink), and  $\text{Y} = \text{Se}$  (purple).

**TABLE 1: QM/MM Energies (in kcal mol<sup>-1</sup>) for the Conversion of Xanthine to Uric Acid, with the Cofactor of XO in the Oxo, Sulfido, and Selenido Form<sup>a</sup>**

	oxo		sulfido			selenido	
	BP86	B3LYP	BP86	B3LYP	BP86	B3LYP	
reactant	0.0	0.0	0.0	0.0	0.0	0.0	
TS1'	2.5 (2.5)	5.6 (5.6)	2.9 (2.9)	8.5 (8.5)	3.1 (3.1)	5.2 (5.2)	
IM1'	-7.4	-7.2	-8.0	-7.5	-8.2	-9.6	
TS1''	-6.9 (0.5)	-7.1 (0.1)	-7.4 (0.6)	-7.2 (0.3)	-7.1 (1.1)	-9.4 (0.2)	
IM1''	-8.9	-9.5	-9.0	-8.6	-8.7	-10.7	
TS1	1.8 (10.7)	1.6 (11.1)	1.0 (10.0)	2.5 (11.1)	0.4 (9.1)	-1.3 (9.4)	
IM1	-1.1	0.7	-3.4	-1.8	-3.1	-3.8	
TS2	-0.5 (0.6)	2.6 (1.9)	-2.1 (1.3)	2.5 (4.3)	-1.0 (2.1)	0.2 (4.0)	
IM2	4.7	0.9	-7.8	-2.5	-6.6	-5.7	
TS3	19.6 (14.9)	21.2 (20.3)	0.7 (8.5)	4.5 (7.0)	0.6 (7.2)	-0.8 (4.9)	
product	6.2	-4.4	-0.8	-9.3	-0.8	-10.7	
$\Delta E_{\max}$	28.5	30.6	10.0	13.1	9.3	10.9	

<sup>a</sup> Activation barriers relative to the preceding minima are given in parentheses.

H—S or H—Se. Overall, TS3 resembles the energetically favored product state more for  $\text{Y} = \text{Se}$  than for  $\text{Y} = \text{O}$ .

**3.2. Influence of the Substrate: 2-Oxo-6-methylpurine.** In the case of xanthine, the reactivity is strongly dependent on the tautomeric form of the substrate.<sup>15</sup> For 2-oxo-6-methylpurine, we investigated four different tautomers that differ in the protonation pattern of the nitrogen atoms of the purine ring; see Figure 3. The electrostatic potential plots for xanthine and

2-oxo-6-methylpurine are quite similar, in spite of the fact that the nitrogen atoms in neutral xanthine carry three protons, instead of two in 2-oxo-6-methylpurine, and regardless of the replacement of the negatively charged O6 atom in the former (acting as a hydrogen bond acceptor) by an essentially neutral methyl group in the latter. For example, tautomer 3 of 2-oxo-6-methylpurine has an electrostatic potential map analogous to tautomer A of xanthine, while tautomer 4 resembles the active

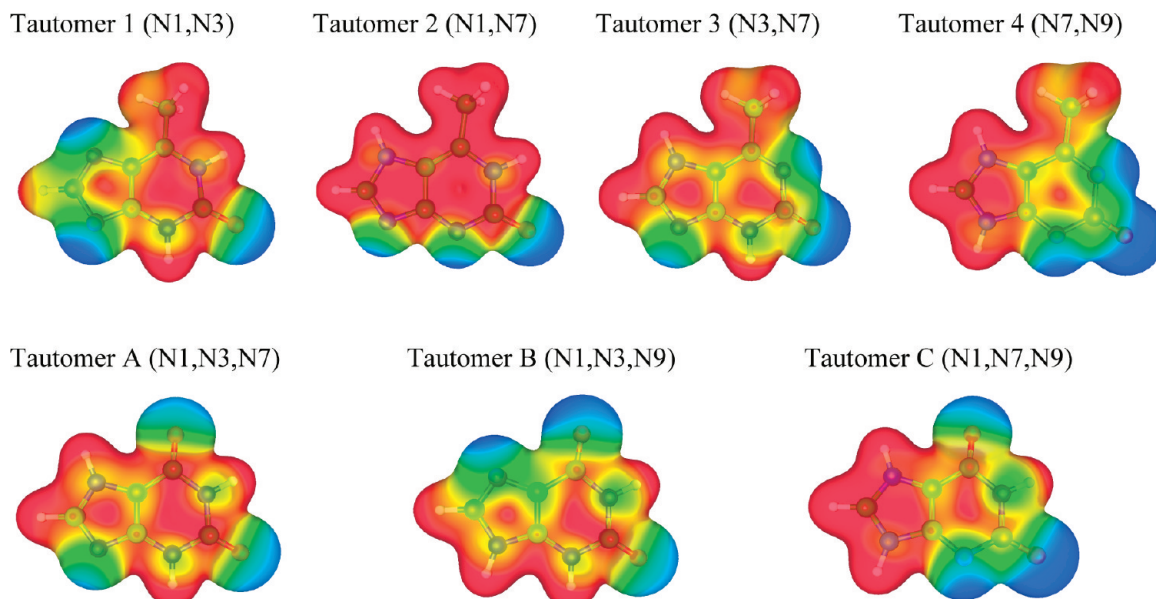


**Figure 3.** Electrostatic potential plots for different tautomers of 2-oxo-6-methylpurine (top panel, tautomers 1–4) and xanthine (bottom panel, tautomers A–C). The electrostatic potential is mapped on a density isosurface (0.01e). Red (blue) indicates a positive (negative) potential.

**TABLE 2: Relative Energies of Tautomers 1–4 of 2-Oxo-6-methylpurine in kcal mol<sup>-1</sup>**

	$\Delta E^a$	$\Delta E^b$	$\Delta E^c$	$\Delta E(\text{COSMO})^d$
tautomer 1	0.0	0.0	0.0	0.0
tautomer 2	11.4	11.2	10.6	0.7
tautomer 3	4.7	4.5	4.1	0.2
tautomer 4	not calculated	33.7	33.0	12.2

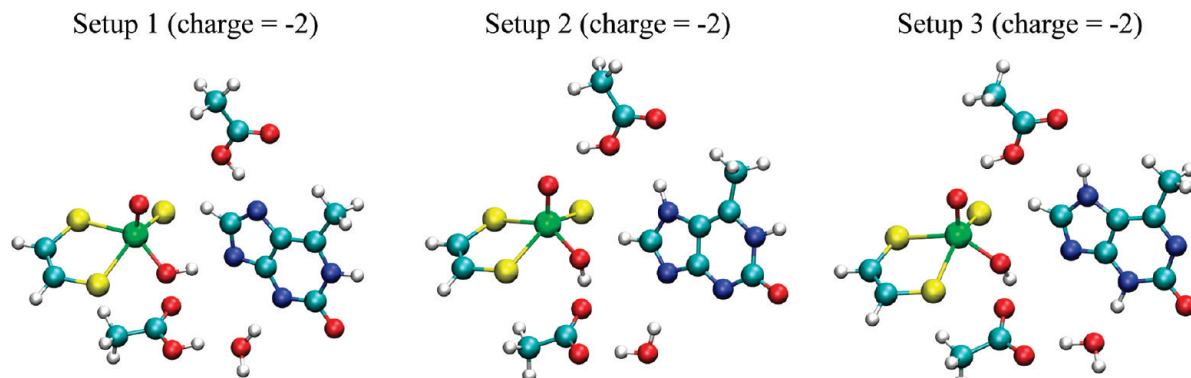
<sup>a</sup> B3LYP/6-31G(d).<sup>64</sup> <sup>b</sup> B3LYP/6-31+G\*\*. <sup>c</sup> B3LYP/def2-TZVP. <sup>d</sup> B3LYP/def2-TZVP,  $\epsilon = 80$ .

xanthine species with a doubly protonated imidazole substructure (tautomer C). Again, as in the case of xanthine,<sup>15</sup> the energies of the four tautomers of 2-oxo-6-methylpurine show a large spread in the gas phase but lie much closer to each other in a continuum (COSMO) solvent where tautomers 1–3 are within 1 kcal mol<sup>-1</sup>; see Table 2. We therefore computed reaction paths for all of these tautomers. The standard QM regions of the starting structures are depicted in Figure 4; the larger QM regions also include Gln767 and Arg880 in the QM part.

**Setup 1 (See Figure S3 in the Supporting Information).** Tautomer 1 is the most stable tautomer in gas-phase calculations. In the enzyme, the lack of a proton at N7 causes coordination by the protonated Glu802 residue. Having two protons at the pyrimidine ring, tautomer 1 is not stable as a neutral species in the binding pocket but immediately transfers its N3 proton to Glu1261 which thus becomes less acidic. Consequently, the hydroxyl group of the cofactor rearranges and establishes a hydrogen bond to N9 of the substrate; see Figure 4. Starting from this reactant state, we could not locate an intermediate in which the proton of the cofactor hydroxyl group is transferred to the substrate without the C–O bond being formed. Instead, these two changes happen at the same time so that we directly obtain a tetrahedral structure as the first intermediate (IM2), which bears a proton at N9 (not at N7), establishing a hydrogen bond with OE1 of Glu1261. The second step is a formal hydride transfer of H8 to the sulfido group of the cofactor.

For both snapshots considered, we generally find good agreement in the computed geometries and relative energies: Both the BP86 and B3LYP functionals assign TS2 as the rate-limiting barrier, although TS3 lies only slightly below TS2. The barrier is somewhat lower for BP86 (about 18 kcal mol<sup>-1</sup>) than for B3LYP (about 23 kcal mol<sup>-1</sup>, rising to 25.8 kcal mol<sup>-1</sup> for the large QM region); see Table 3. These values are higher than the barrier derived from experimental data: Using the Eyring equation<sup>65</sup> to convert the reported values for the rate constant of  $k_{\text{red}} = 57 \text{ s}^{-1}$ ,<sup>13</sup> the resulting experimental barrier is 14.8 kcal mol<sup>-1</sup>.

**Setup 2 (See Figure S4 in the Supporting Information).** Using the standard QM region, the reactant state of the (N1, N7) tautomer 2 can be optimized in the enzyme only for snapshot SN400, whereas it rearranges spontaneously to the intermediate IM1 in the case of snapshot SN200. This rearrangement involves a double proton transfer: one proton is shifted from Glu802 to the oxo ligand of the cofactor to form an apical hydroxyl group, and another proton from the equatorial hydroxyl group is transferred to Glu1261. This supports the suggestion<sup>24</sup> that deprotonation of the cofactor is induced by substrate binding. Note that the initial rearrangement differs slightly in SN400 with the large QM region where Gln767 is a QM residue and can thus act as a hydrogen bond acceptor. Considering the reaction pathways from IM1 onward, there are again slight differences between the two snapshots. In the course of C–O bond formation, the proton is transferred back in SN200 from the apical hydroxyl group of the cofactor directly to Glu802, whereas this happens in two distinct steps in SN400. However, the overall transformation is the same in both snapshots. The last step is a combined proton-hydride transfer, in which the hydrogen atom H8 of the substrate migrates to the sulfido group of the cofactor while the proton at N9 is concomitantly transferred back to Glu1261. The extent of proton transfer in the corresponding transition state depends on the functional used: the proton is already transferred to Glu1261 with BP86 (OE2–H bond length: 1.03 Å), whereas it still resides

**Figure 4.** Standard QM regions of the three chosen setups for 2-oxo-6-methylpurine: reactant states of tautomers 1–3.**TABLE 3: QM/MM Energies of Different Snapshots in kcal mol<sup>-1</sup> Calculated for Setup 1 of 2-Oxo-6-methylpurine, Relative to the Energy of the Reactant<sup>a</sup>**

	SN200-BP86	SN200-B3LYP	SN400-BP86	SN400-B3LYP	SN400-B3LYP, large QM
reactant	0.0	0.0	0.0	0.0	0.0
TS2	18.1 (18.1)	22.7 (22.7)	17.6 (17.6)	23.4 (23.4)	25.8 (25.8)
IM2	12.2	17.7	10.4	16.0	20.0
TS3	17.6 (5.4)	22.6 (4.9)	15.6 (5.2)	21.7 (5.7)	24.3 (4.3)
product	13.7	7.5	11.1	6.0	8.1
$\Delta E_{\text{max}}$	18.1	22.7	17.6	23.4	25.8

<sup>a</sup> Activation barriers relative to the preceding minima are given in parentheses.

**TABLE 4: QM/MM Energies of Different Snapshots in kcal mol<sup>-1</sup> Calculated for Setup 2 of 2-Oxo-6-methylpurine, Relative to the Energy of IM1 (Relative to the Reactant for the Large QM Region)<sup>a</sup>**

	SN200-BP86		SN200-B3LYP		SN400-BP86		SN400-B3LYP		SN400-B3LYP, large QM region	
reactant					4.4		3.9		0.0	
TS1					5.8	(1.4)	7.3	(3.4)	5.8	(5.8)
IM1	0.0		0.0		0.0		0.0		1.4	
TS2	8.7	(8.7)	9.8	(9.8)	8.5	(8.5)	11.6	(11.6)	7.3	(5.9)
IM2	-0.5		-1.1		0.2		1.0		1.9	
TS2'					2.2	(2.0)	4.6	(3.6)	6.6	(4.7)
IM2'					0.7		3.3		1.8	
TS3	5.4	(5.9)	9.3	(10.4)	5.1	(4.4)	11.2	(7.9)	7.0	(5.2)
product	4.3		-5.7		1.3		-7.7		-7.4	
$\Delta E_{\max}$	8.7		10.4		8.5		11.6		7.3	

<sup>a</sup> Activation barriers relative to the preceding minima are given in parentheses.

**TABLE 5: QM/MM Energies of Different Snapshots in kcal mol<sup>-1</sup> Calculated for Setup 3 of 2-Oxo-6-methylpurine, Relative to the Energy of IM1 (IM1' for the Large QM Region)<sup>a</sup>**

	SN200-BP86		SN200-B3LYP		SN400-BP86		SN400-B3LYP		SN400-B3LYP, large QM region	
reactant	9.4		8.3		12.1		9.1		8.9	
TS1'	12.2	(2.7)	13.3	(5.0)	12.7	(0.6)	9.5	(0.4)	11.3	(2.4)
IM1'	3.9		1.8		3.9		1.0		0.0	
TS1	4.6	(0.7)	5.5	(3.7)	5.8	(1.9)	6.5	(5.5)	6.5	(6.5)
IM1	0.0		0.0		0.0		0.0		0.9	
TS2	6.7	(0.3)	9.6	(2.5)	5.9	(0.4)	7.4	(1.5)	9.8	(8.9)
IM2	1.1		3.9		0.6		2.0		5.9	
TS3	8.1	(7.0)	8.9	(5.0)	6.7	(6.1)	7.0	(5.0)	11.3	(5.4)
product	7.9		-1.6		4.4		-6.6		-2.8	
$\Delta E_{\max}$	8.1		8.9		6.7		7.4		11.3	

<sup>a</sup> Activation barriers relative to the preceding minima are given in parentheses.

at the substrate with B3LYP (N9–H bond length: 1.05 Å), which gives a higher barrier for this step. Looking at the overall reaction profile, the barriers for C–O bond formation and hydride transfer are rather similar in the case of B3LYP, the former one being slightly higher and thus rate-determining. Compared with setup 1, the computed barriers for the individual reaction steps are significantly lower in setup 2. This holds especially for the B3LYP results with the large QM region where the highest point on the reaction profile drops to 7.3 kcal mol<sup>-1</sup> (see Table 4), i.e., even below the experimental barrier.

**Setup 3 (See Figure S5 in the Supporting Information).** Initially, the (N3, N7) tautomer 3 is converted into the (N7, N9) tautomer 4 as follows. The proton at N3 is transferred via the crystal water molecule CRYW224 toward Glu1261, and at the same time, the hydroxyl group of the cofactor reorients and establishes a hydrogen bond with the N9 atom of 2-oxo-6-methylpurine. Thereafter, the proton of this hydroxyl group is transferred to the N3 atom of the substrate, and concomitantly, the apical oxygen atom of the cofactor becomes strongly acidic and captures the proton from Glu802 to form an apical hydroxyl group. The thus formed activated tautomer 4 reacts with the cofactor under C–O bond formation, and the resulting tetrahedral intermediate then undergoes a hydride transfer that generates the product.

Both functionals assign IM1 as the Michaelis complex, but they show minor differences in the reaction profiles for C–O bond formation and hydride transfer: For the standard QM region, the latter (former) is assigned to be rate-limiting with BP86 (B3LYP). This can be rationalized by the stronger stabilization of the Mo(IV) product in B3LYP compared with BP86 (by 7–8 kcal mol<sup>-1</sup>) which leads to an “earlier” transition state for the hydride transfer (with a slightly lower energy). The key C8–H8 distance in the transition state is 1.60–1.65 Å in

the two BP86 snapshots and 1.42 Å in both B3LYP snapshots. However, one should emphasize that the energetic differences are small (less than 2 kcal mol<sup>-1</sup>, see Table 5) and thus not very relevant. According to B3LYP, the highest point on the reaction profile is at 7.4–9.6 kcal mol<sup>-1</sup> for the two chosen snapshots (rising to 11.3 kcal mol<sup>-1</sup> for SN400 with the larger QM region, see Table 5).

**QM Model Study (Figure 5).** To examine the intrinsic reactivity of 2-oxo-6-methylpurine compared to xanthine, we performed a QM study on a minimal gas-phase model consisting of parts of the cofactor and the substrate; see Table 6. For both substrates, we find a three-step mechanism, involving a proton transfer (via TS1), C–O bond formation (via TS2), and a final hydride transfer (via TS3). Considering the rate-limiting final step, the barrier relative to the preceding minimum (IM2) is lower for xanthine, but the overall barrier  $\Delta E_{\max}$  is lower for 2-oxo-6-methylpurine due to the stronger stabilization of IM2 by 4.6 kcal mol<sup>-1</sup>. It should, however, be noted that the QM and QM/MM mechanisms differ, since the QM model system does not include Glu802, so that it is impossible to form an apical OH group.

**Summary.** The overall barrier for setup 1 is considerably larger than those for setups 2 and 3, and also much too high compared with experiment.<sup>13</sup> Hence, tautomer 1 of 2-oxo-6-methylpurine (which is the most stable one in the gas phase) can be excluded as the reactive species in the enzyme, in analogy to the case of xanthine. The overall barriers for setups 2 and 3 are of comparable size, i.e., slightly lower for 2 (3) when using the large (standard) QM region, so that both pathways appear feasible. The overall B3LYP/MM barriers for the various snapshots in these two setups lie between 7.3 and 11.6 kcal mol<sup>-1</sup> and are thus somewhat lower than the value of 14.8 kcal mol<sup>-1</sup> derived from experiment (see above). Compared with

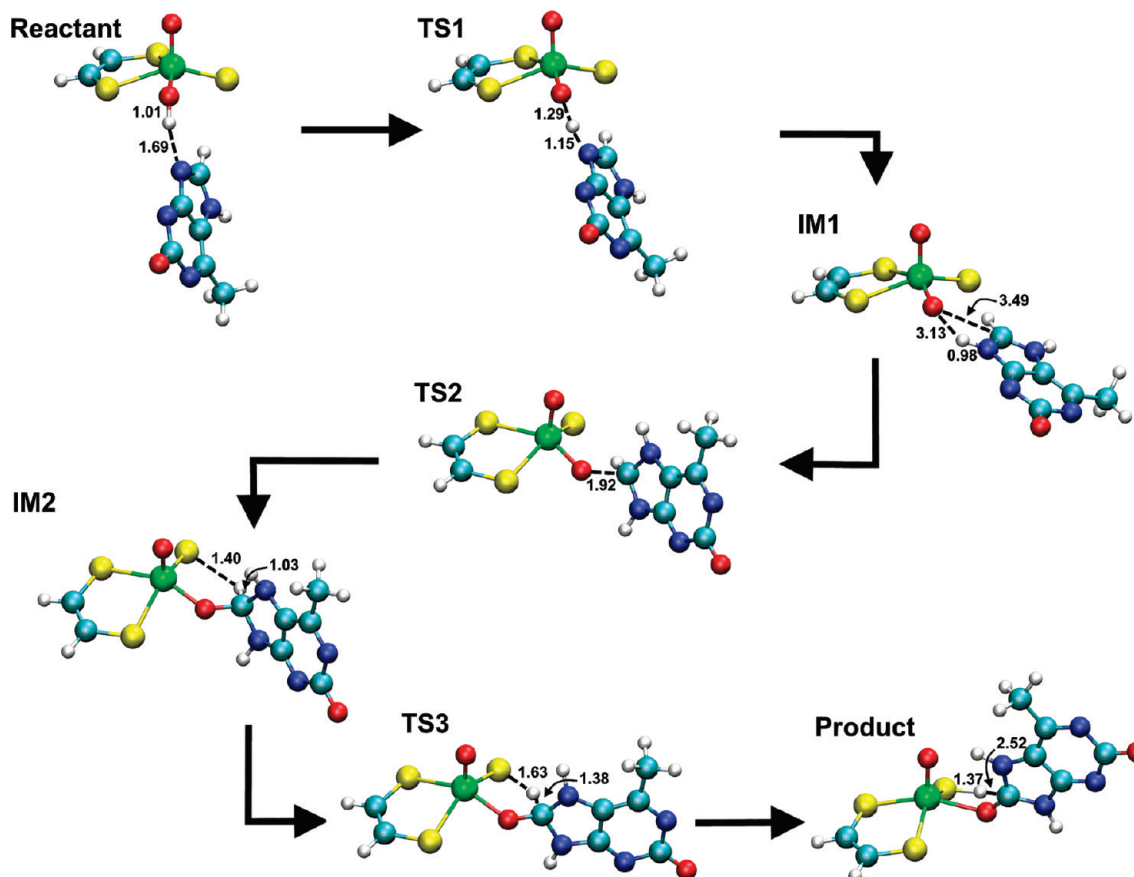


**Figure 5.** Reaction mechanism obtained from the QM model study of 2-oxo-6-methylpurine.

**TABLE 6: QM Energies for the Gas-Phase Calculations on Setup 3 of 2-Oxo-6-methylpurine in kcal mol<sup>-1</sup>, Relative to the Energy of the Reactant<sup>a</sup>**

	2-oxo-6-methylpurine	xanthine <sup>15</sup>
reactant (IM1) <sup>15</sup>	0.0	0.0
TS1	4.6 (4.6)	5.5 (5.5)
IM1	3.0	5.4
TS2	11.2 (8.2)	15.4 (10.0)
IM2	6.2	10.8
TS3	13.4 (7.2)	16.8 (6.0)
product	-17.4	-13.3
$\Delta E_{\max}$	13.4	16.8

<sup>a</sup> Activation barriers relative to the preceding minima are given in parentheses.

xanthine (B3LYP/MM barriers of 13–15 kcal mol<sup>-1</sup>), 2-oxo-6-methylpurine should thus be oxidized more easily by XO, consistent with the calculated intrinsic gas-phase reactivity of these two substrates (see above). Experimentally, the catalytic conversion of 2-oxo-6-methylpurine in XO is only slightly faster than that of xanthine, by a factor of about 10. We note again in this context that 2-oxo-6-methylpurine is considered a “slow” substrate only because of the sluggish product release.<sup>13</sup>

**3.3. Influence of the Glu802 → Gln Mutation.** Our recent QM/MM study<sup>15</sup> on the conversion of xanthine to uric acid in xanthine oxidase showed the essential mechanistic role of Glu1261 and Arg880, for activating the cofactor and for stabilizing the crucial intermediates and transition states, respectively, whereas Glu802 mainly acted as a spectator on the favored pathway (setup G). On the other hand, Glu802 strongly affects the reactivity when hypoxanthine is used as a substrate,<sup>12</sup> and it may have some influence on the different

orientations observed for xanthine and 2-oxo-6-methylpurine in the binding pocket.<sup>8,17</sup>

In the case of xanthine, the pathway with an “upside” orientation of the substrate and deprotonated Glu802 was found to have a barrier of at least 40 kcal mol<sup>-1</sup> which is lowered to about 20 kcal mol<sup>-1</sup> in the presence of protonated Glu802.<sup>15</sup> In the latter case, the substrate is able to change from the (N1, N3, N7) to the (N1, N7, N9) tautomer by using Glu802 as a proton shuttle.<sup>15</sup> This functionality should vanish for a Glu802 → Gln mutation which we investigate here.

Recently published kinetic data for the corresponding mutant of XDH show the overall rate constant to drop from  $k_{\text{cat}} = 108$

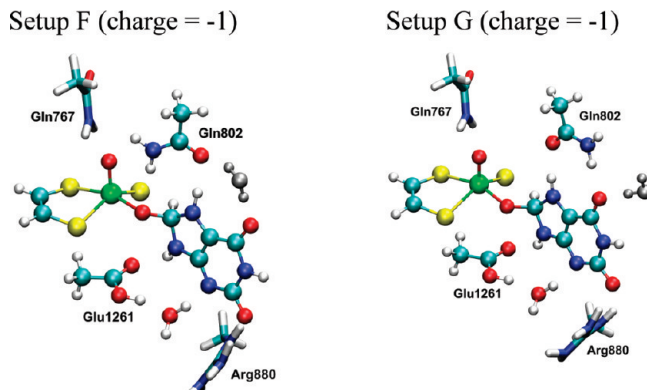


**Figure 6.** QM regions of the two chosen setups F and G for the mutant. For consistency reasons, we use the same notation as in our previous publication.<sup>15</sup> The standard QM region is shown in ball-and-stick representation, whereas the large QM region also contains Gln767 and Arg880 but excludes the water molecule colored in gray.

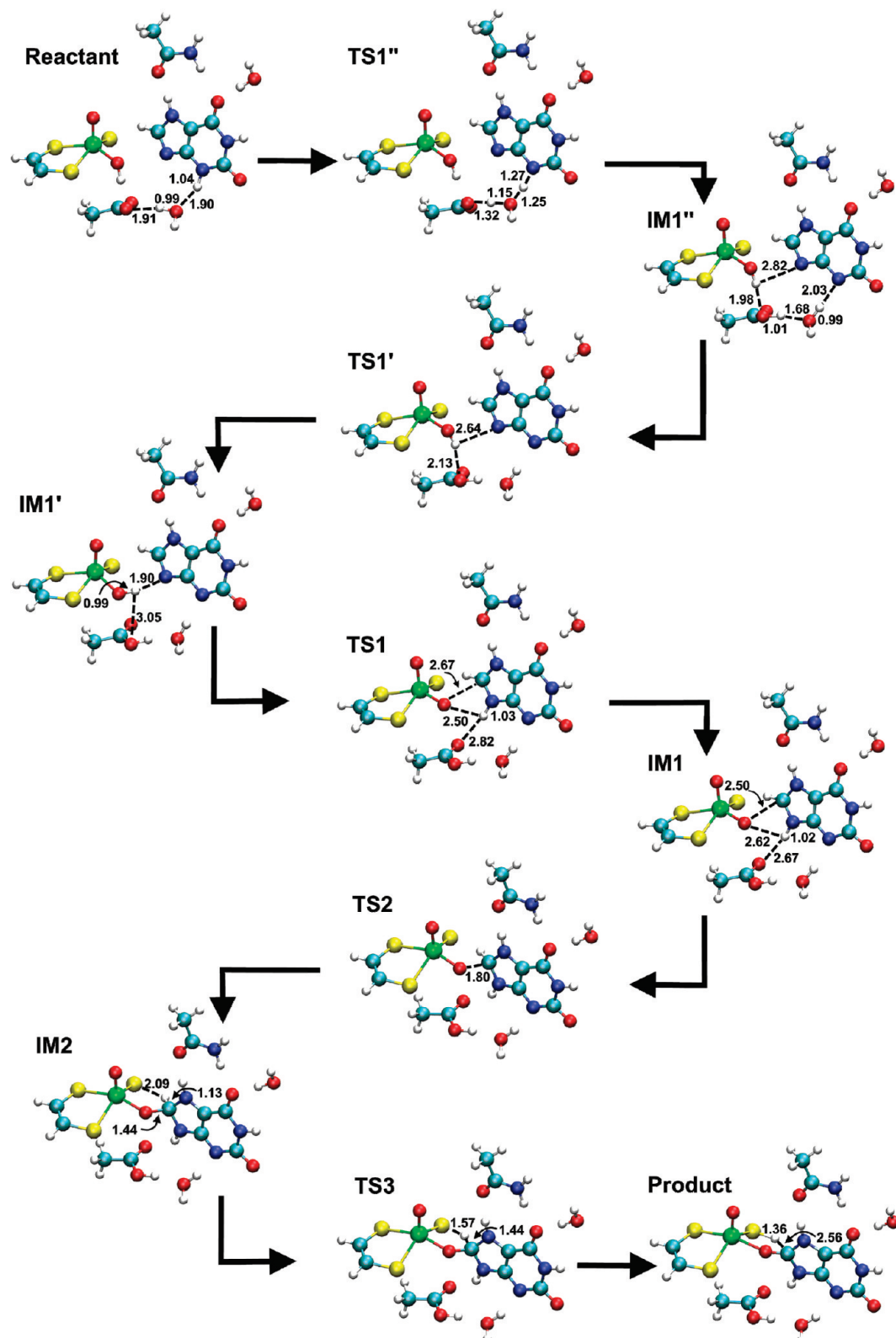


**Figure 7.** Reaction mechanism for the oxidation of xanthine in the mutant: setup G (SN400).

$\pm 1.5 \text{ s}^{-1}$  for the wild-type enzyme to  $1.16 \pm 0.08 \text{ s}^{-1}$  for the mutant.<sup>31</sup> This decrease by a factor of 90 implies an increase in the Eyring activation energy of  $2.5 \text{ kcal mol}^{-1}$ . We examine whether we find a similar effect of this mutation in XO, using two different setups F and G (see Figure 6, same notation as in our previous publication<sup>15</sup>).

Since setup G had been preferred in the wild-type enzyme, we used it as an obvious starting point for the mutant and indeed

obtained essentially the same reaction pathway; see Figure 7. The barriers for the individual steps are similar in both cases, but the intermediates IM1 and IM2 are destabilized in the mutant, by  $2.7$  and  $5.3 \text{ kcal mol}^{-1}$  relative to the wild-type enzyme (see Table 7), which leads to an increase of the overall barrier to  $17.5 \text{ kcal mol}^{-1}$ . For the large QM region, IM2 is further destabilized by another  $3.6 \text{ kcal mol}^{-1}$ , and the overall barrier becomes  $22.0 \text{ kcal mol}^{-1}$ . We crosschecked and con-

**TABLE 7: QM/MM Energies in kcal mol<sup>-1</sup> Calculated for Setup G (SN 400), Relative to the Energy of Intermediate IM1<sup>a</sup>**

	SN400	SN400, Gln802	SN400, Gln802, large QM
reactant	8.7	9.1	9.0
TS1''	17.2 (8.5)	16.0 (6.9)	16.7 (16.7)
IM1''	1.2	2.5	5.5
TS1'	1.5 (0.3)	2.5 (0.0)	5.7 (0.2)
IM1'	0.0	0.0	0.0
TS1	11.1 (11.1)	11.3 (11.3)	10.6 (10.6)
IM1	6.8	9.5	9.6
TS2	11.1 (4.3)	15.1 (5.6)	18.3 (8.7)
IM2	6.2	11.5	15.1
TS3	13.2 (7.0)	17.5 (6.0)	22.0 (6.9)
product	-0.6	2.7	7.6
$\Delta E_{\text{max}}$	13.1	17.5	22.0

<sup>a</sup> The three columns give the values for the wild-type enzyme, the Glu802 → Gln mutant using the standard QM region, and the mutant using the large QM region, respectively. Activation barriers relative to the preceding minima are given in parentheses.

firmed these results for snapshot SN100 where we obtained overall barriers of 18.2 (24.2) kcal mol<sup>-1</sup> for the standard (large) QM region.

In the mutant, the computed barrier for setup G is thus significantly higher than that in the wild-type enzyme, and it also considerably exceeds the experimental value. The high barrier is mainly due to the destabilization of IM2, caused by an accumulation of charge on O6. This could be alleviated by a rotation of Gln802 (as in setup F) that would allow a water molecule to coordinate to O6 and thus provide some stabilization.

Therefore, we investigated setup F as an alternative. We again find very similar reaction pathways for the wild-type enzyme and the mutant; see Figure 8. There is, however, one essential difference: The intermediate IM1 is much less stable in the mutant compared with the wild-type enzyme, by more than 11 kcal mol<sup>-1</sup>, since the stabilizing proton transfer (from Glu802) is no longer possible in the Glu802 → Gln802 mutant. The potential surface is thus generally flatter in the mutant, with an overall barrier of 15.8 (17.1) kcal mol<sup>-1</sup> for the standard (large) QM region in snapshot SN400. The corresponding values for

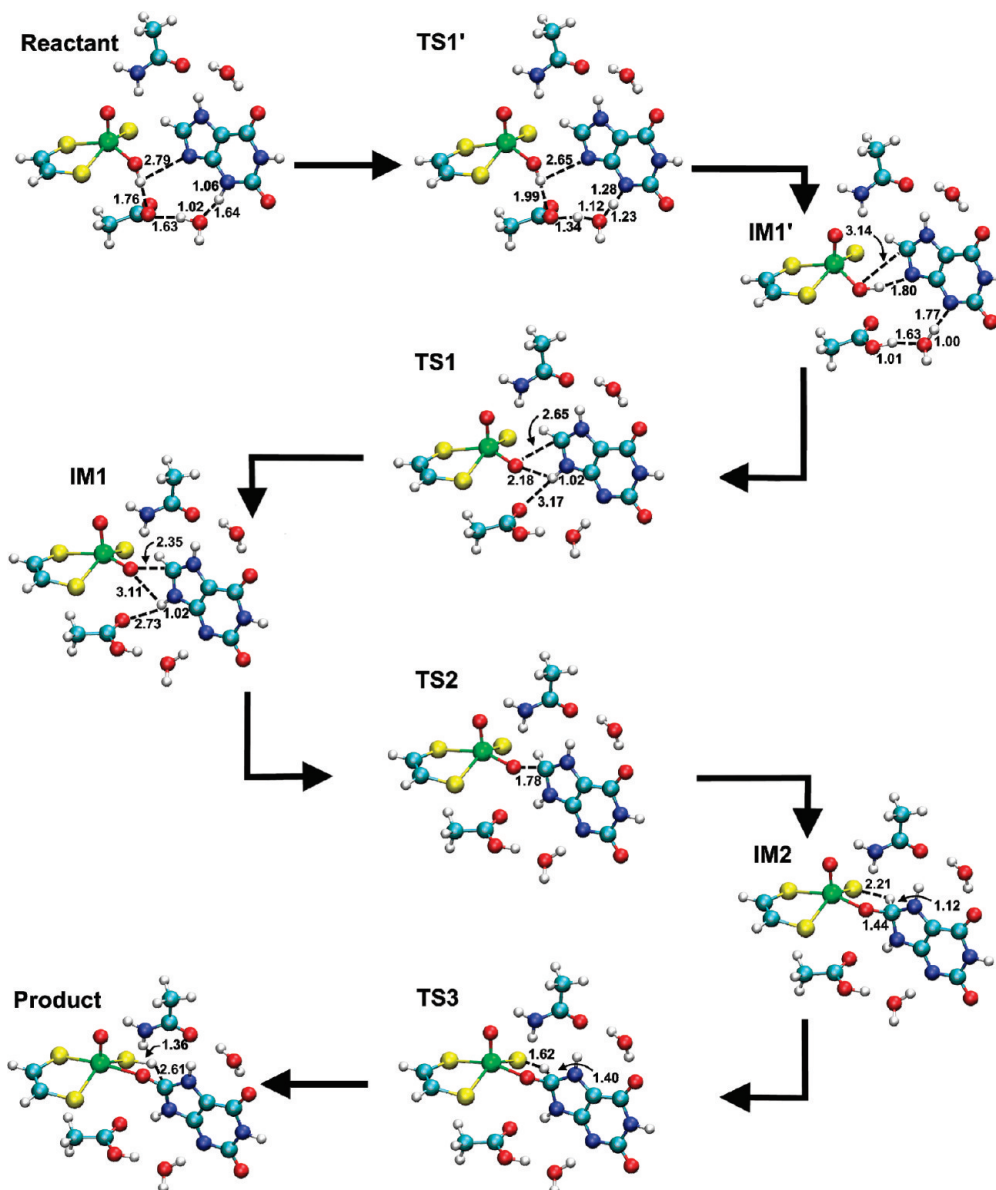


**Figure 8.** Reaction mechanism for the oxidation of xanthine in the mutant: setup F (SN400).

**TABLE 8: QM/MM Energies in kcal mol<sup>-1</sup> Calculated for Setup F (SN400), Relative to the Energy of the Intermediate IM1'**<sup>a</sup>

	SN400	SN400, Gln802	SN400, Gln802, large QM
reactant	9.4	9.1	7.7
TS1'	13.6 (4.2)	12.0 (2.9)	11.8 (4.1)
IM1'	0.0	0.0	0.0
TS1	9.0 (9.0)	9.8 (9.8)	9.6 (9.6)
IM1	-3.7	7.7	7.6
TS2	15.4 (19.1)	13.1 (5.3)	14.9 (7.3)
IM2	11.4	10.3	10.4
TS3	16.6 (5.2)	15.8 (5.5)	17.1 (6.7)
product	0.3	-3.7	-2.9
$\Delta E_{\max}$	20.3	15.8	17.1

<sup>a</sup> The three columns give the values for the wild-type enzyme, the Glu802 → Gln mutant with the standard QM region, and the mutant with the large QM region, respectively. Activation barriers relative to the preceding minima are given in parentheses.

snapshot SN100 are somewhat higher, i.e., 19.6 (21.3) kcal mol<sup>-1</sup> (see Table 8).

Following the same procedure as in our previous QM/MM study,<sup>15</sup> we performed cluster QM calculations<sup>66–69</sup> in an attempt to establish to a common energy scale for the different setups and snapshots (including all residues shown in Figure 6 in the QM cluster and representing the environment of the cluster by a polarizable continuum with a dielectricity constant of  $\epsilon = 8$ ). According to these cluster calculations, the reactants of the closely related setups F and G are essentially isoenergetic and should thus both be populated at room temperature. Hence, the results for these two setups are directly comparable with each other. For the standard QM region, the preferred pathway in the Glu802 → Gln mutant is setup F with an overall B3LYP/MM barrier of 15.8 kcal mol<sup>-1</sup> for the conversion of xanthine to uric acid, while the corresponding best B3LYP/MM value (analogous QM region) in the wild-type enzyme is 13.1 kcal mol<sup>-1</sup> (setup G). In the case of XO, the calculations thus predict an increase in the barrier of 2.7 kcal mol<sup>-1</sup> upon mutation, in

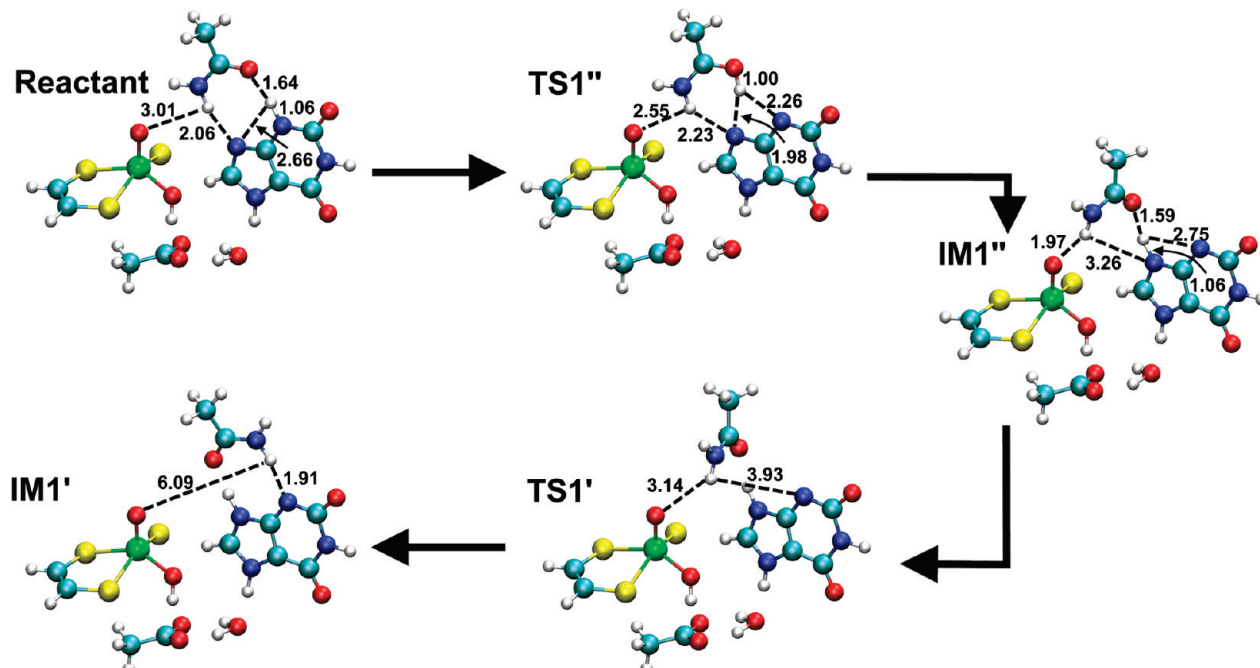
**TABLE 9: QM/MM Energies in kcal mol<sup>-1</sup> Calculated for Setup A, Relative to the Energy of the Reactant<sup>a</sup>**

	SN500	SN500, Gln802	SN500, Gln802, large QM
reactant	0.0	0.0	0.0
TS1''		20.0 (20.0)	19.9 (19.9)
IM1''		7.1	10.0
TS1'	8.9 (8.9)	15.9 (8.8)	17.6 (7.6)
IM1'	2.4	3.7	4.9
TS1	19.1 (16.7)		
IM1	14.9	18.1	18.1
TS2	20.3 (5.4)		
IM2	16.4	19.4	21.0
TS3	21.7 (5.3)	23.9 (4.5)	25.7 (4.7)
product	0.5	3.7	3.7
$\Delta E_{\max}$	21.7	23.9	25.7

<sup>a</sup> The three columns give the values for the wild-type enzyme, the Glu802 → Gln mutant with the standard QM region, and the mutant with the large QM region. Activation barriers relative to the preceding minima are given in parentheses.

good accord with the experimental value of 2.5 kcal mol<sup>-1</sup> for XDH.<sup>31</sup> More important than this partly fortuitous numerical agreement is the qualitative conclusion that the mutation induces a change in the favored reaction channel from setup G (for the wild-type enzyme) to setup F (for the Glu802 → Gln mutant).

For setups F and G with an “upside down” orientation of the substrate, the initial proton transfer from the N3 to the N9 position is not affected by the mutation of Glu802. This is quite different in the previously proposed alternative “upside” orientation<sup>8,9,17</sup> where the proton shuttle is strongly affected by the Glu802 → Gln mutation. In the corresponding setup A, the proton transfer now occurs in two separate steps (see Figure 9). The proton at N3 first moves to N9, being bound to Gln802 in the transition state. In the resulting intermediate (IM1''), the amide group of Gln802 is coordinated to the cofactor, and a simple rotation of the Gln802 side chain is needed to affect coordination of the amide group to the substrate (thus generating the same bonding situation as in the wild-type enzyme). The barrier for this two-step proton transfer in the mutant (setup A)

**Figure 9.** Part of the reaction mechanism for the oxidation of xanthine in the mutant: setup A (SN100).

is quite high (20 kcal mol<sup>-1</sup> compared to 8.9 kcal mol<sup>-1</sup> in the wild-type enzyme). However, the rate-limiting step is still the hydride transfer reaction, and the influence on the overall barrier is relatively small (+2.2 kcal mol<sup>-1</sup>); see Table 9.

To summarize, the results for the Glu802 → Gln mutant confirm the “upside down” orientation of the substrate in the kinetically active species, since the computed overall barriers for setup F (“upside down”) are much lower than those for setup A (“upside”), typically by 8–9 kcal mol<sup>-1</sup>.

#### 4. Conclusions

We have extended our previous QM/MM study of the reductive half-reaction of xanthine oxidase by considering variations of the cofactor, the substrate, and the active-site Glu802 residue. The present calculations confirm that the enzyme becomes inactive when the sulfido ligand in the cofactor is replaced by an oxo ligand, while selenido substitution is predicted to increase the activity by lowering the overall barrier. For the alternative substrate 2-oxo-6-methylpurine, we determined the reaction mechanisms for three different tautomers (two snapshots each) and obtained overall barriers (B3LYP/CHARMM, large QM region) of 25.8, 7.3, and 11.3 kcal mol<sup>-1</sup>, respectively. Therefore, only the latter two pathways are viable which involve tautomers 2–4 rather than the lowest-energy gas-phase tautomer 1. Our results agree with the experimental finding that the conversion of the Michaelis complex to the product complex is more facile when using 2-oxo-6-methylpurine instead of xanthine as a substrate. QM model studies also indicate an intrinsically higher reactivity of 2-oxo-6-methylpurine compared with xanthine. In each case, the most favorable pathway involves the “upside down” orientation of the substrate in the binding pocket, contrary to previous claims that the differences in reactivity may be caused by different substrate orientations.

For the Glu802 → Gln mutant, we investigated two competing pathways with “upside down” substrate orientation that had also been studied previously for the wild-type enzyme (setups F and G). These pathways differ mainly in the orientation of the Glu802/Gln802 residue. The mutant and the wild-type enzyme prefer different mechanisms (F and G, respectively) for two reasons. First, setup F is disfavored in the wild-type enzyme, since the intermediate IM1 acts as a thermodynamic sink, being stabilized by a proton transfer from Glu802 which is not possible in the mutant (containing Gln802), and therefore, the overall energy profile is flatter in the mutant and has a lower overall barrier. Second, setup G is disfavored in the mutant, because the negative charge developing at the O6 position during the reaction is less well stabilized by Gln802 compared with Glu802. The computed differences in the overall barriers for wild-type XO (setup G) and the Glu802 → Gln mutant (setup F) are in accord with corresponding experimental data for XDH. For the “upside” orientation of the substrate in the mutant (setup A), the barriers are calculated to be much higher (by 8–9 kcal mol<sup>-1</sup>), again in analogy to wild-type XO.<sup>15</sup>

In summary, the present results are consistent with the stepwise mechanism and the substrate orientation proposed in our previous QM/MM studies and with the available experimental results for the examined variations of cofactor, substrate, and active-site residue.

**Acknowledgment.** This work was supported by the Max-Planck-Gesellschaft. S.M. thanks the Fonds der Chemischen Industrie for a Kekulé scholarship.

**Supporting Information Available:** System setup; CHARMM parameters; QM, MM, and QM/MM energies of all stationary points; and complete refs 32, 36, and 55. This material is available free of charge via the Internet at <http://pubs.acs.org>.

#### References and Notes

- (1) Hille, R. *Chem. Rev.* **1996**, *96*, 2757–2816.
- (2) Schardinger, F. Z. *Unters. Nahr. Genussm.* **1902**, *5*, 1113–1121.
- (3) Massey, V.; Harris, C. M. *Biochem. Soc. Trans.* **1997**, *25*, 750–755.
- (4) Hille, R.; Sprecher, H. *J. Biol. Chem.* **1987**, *262*, 10914–10917.
- (5) Romão, M. J.; Archer, M.; Moura, I.; Moura, J. J. G.; Legall, J.; Engh, R.; Schneider, M.; Hof, P.; Huber, R. *Science* **1995**, *270*, 1170–1176.
- (6) Huber, R.; Hof, P.; Duarte, R. O.; Moura, J. J. G.; Moura, I.; Liu, M. Y.; LeGall, J.; Hille, R.; Archer, M.; Romão, M. J. *Proc. Natl. Acad. Sci. U.S.A.* **1996**, *93*, 8846–8851.
- (7) Okamoto, K.; Matsumoto, K.; Hille, R.; Eger, B. T.; Pai, E. F.; Nishino, T. *Proc. Natl. Acad. Sci. U.S.A.* **2004**, *101*, 7931–7936.
- (8) Pauff, J. M.; Hemann, C. F.; Jüinemann, N.; Leimkühler, S.; Hille, R. *J. Biol. Chem.* **2007**, *282*, 12785–12790.
- (9) Pauff, J. M.; Zhang, J. J.; Bell, C. E.; Hille, R. *J. Biol. Chem.* **2008**, *283*, 4818–4824.
- (10) Kim, J. H.; Ryan, M. G.; Knaut, H.; Hille, R. *J. Biol. Chem.* **1996**, *271*, 6771–6780.
- (11) Choi, E. Y.; Stockert, A. L.; Leimkühler, S.; Hille, R. *J. Inorg. Biochem.* **2004**, *98*, 841–848.
- (12) Yamaguchi, Y.; Matsumura, T.; Ichida, K.; Okamoto, K.; Nishino, T. *J. Biochem.* **2007**, *141*, 513–524.
- (13) McWhirter, R. B.; Hille, R. *J. Biol. Chem.* **1991**, *266*, 23724–23731.
- (14) Metz, S.; Wang, D.; Thiel, W. *J. Am. Chem. Soc.* **2009**, *131*, 4628–4640.
- (15) Metz, S.; Thiel, W. *J. Am. Chem. Soc.* **2009**, *131*, 14885–14902.
- (16) Mondal, M. S.; Mitra, S. *Biochemistry* **1994**, *33*, 10305–10312.
- (17) Pauff, J. M.; Cao, H.; Hille, R. *J. Biol. Chem.* **2009**, *284*, 8760–8767.
- (18) Truglio, J. J.; Theis, K.; Leimkühler, S.; Rappa, R.; Rajagopalan, K. V.; Kisker, C. *Structure* **2002**, *10*, 115–125.
- (19) Bray, M. R.; Deeth, R. *J. J. Chem. Soc., Dalton Trans.* **1997**, 4005–4009.
- (20) Voityuk, A. A.; Albert, K.; Romão, M. J.; Huber, R.; Rösch, N. *Inorg. Chem.* **1998**, *37*, 176–180.
- (21) Zhang, X. H.; Wu, Y. D. *Inorg. Chem.* **2005**, *44*, 1466–1471.
- (22) Illich, P.; Hille, R. *J. Phys. Chem. B* **1999**, *103*, 5406–5412.
- (23) Illich, P.; Hille, R. *J. Am. Chem. Soc.* **2002**, *124*, 6796–6797.
- (24) Amano, T.; Ochi, N.; Sato, H.; Sakaki, S. *J. Am. Chem. Soc.* **2007**, *129*, 8131–8138.
- (25) Bayse, C. A. *Dalton Trans.* **2009**, 2306–2314.
- (26) Massey, V.; Edmondson, D. *J. Biol. Chem.* **1970**, *245*, 6595–6598.
- (27) Wagener, N.; Pierik, A. J.; Ibdah, A.; Hille, R.; Dobbek, H. *Proc. Natl. Acad. Sci. U.S.A.* **2009**, *106*, 11055–11060.
- (28) Bray, R. C.; George, G. N. *Biochem. Soc. Trans.* **1985**, *13*, 560–567.
- (29) Xia, M.; Illich, P.; Dempski, R.; Hille, R. *Biochem. Soc. Trans.* **1997**, *25*, 768–773.
- (30) Leimkühler, S.; Stockert, A. L.; Igarashi, K.; Nishino, T.; Hille, R. *J. Biol. Chem.* **2004**, *279*, 40437–40444.
- (31) Dietzel, U.; Kuper, J.; Doeblner, J. A.; Schulten, A.; Truglio, J. J.; Leimkühler, S.; Kisker, C. *J. Biol. Chem.* **2009**, *284*, 8768–8776.
- (32) MacKrell, A. D.; et al. *J. Phys. Chem. B* **1998**, *102*, 3586–3616.
- (33) Brooks, B. R.; Bruccoleri, R. E.; Olafson, B. D.; States, D. J.; Swaminathan, S.; Karplus, M. *J. Comput. Chem.* **1983**, *4*, 187–217.
- (34) Luo, G. B.; Andricioaei, I.; Xie, X. S.; Karplus, M. *J. Phys. Chem. B* **2006**, *110*, 9363–9367.
- (35) Billeter, S. R.; Turner, A. J.; Thiel, W. *Phys. Chem. Chem. Phys.* **2000**, *2*, 2177–2186.
- (36) Sherwood, P.; et al. *THEOCHEM* **2003**, *632*, 1–28.
- (37) Ahlrichs, R.; Bär, M.; Häser, M.; Horn, H.; Kölmel, C. *Chem. Phys. Lett.* **1989**, *162*, 165–169.
- (38) Smith, W.; Forester, T. R. *J. Mol. Graphics* **1996**, *14*, 136–141.
- (39) Bakowies, D.; Thiel, W. *J. Phys. Chem.* **1996**, *100*, 10580–10594.
- (40) de Vries, A. H.; Sherwood, P.; Collins, S. J.; Rigby, A. M.; Rigitto, M.; Kramer, G. *J. Phys. Chem. B* **1999**, *103*, 6133–6141.
- (41) Sherwood, P.; de Vries, A. H.; Collins, S. J.; Greatbanks, S. P.; Burton, N. A.; Vincent, M. A.; Hillier, I. H. *Faraday Discuss.* **1997**, *79*–92.
- (42) Klamt, A.; Schürmann, G. *J. Chem. Soc., Perkin Trans. 2* **1993**, *5*, 799–805.
- (43) Slater, J. C. *Phys. Rev.* **1951**, *81*, 385–390.
- (44) Vosko, S. H.; Wilk, L.; Nusair, M. *Can. J. Phys.* **1980**, *58*, 1200–1211.

- (45) Becke, A. D. *Phys. Rev. A* **1988**, *38*, 3098–3100.
- (46) Perdew, J. P. *Phys. Rev. B* **1986**, *33*, 8822–8824.
- (47) Perdew, J. P. *Phys. Rev. B* **1986**, *34*, 7406.
- (48) Eichkorn, K.; Treutler, O.; Öhm, H.; Häser, M.; Ahlrichs, R. *Chem. Phys. Lett.* **1995**, *240*, 283–289.
- (49) Eichkorn, K.; Weigend, F.; Treutler, O.; Ahlrichs, R. *Theor. Chem. Acc.* **1997**, *97*, 119–124.
- (50) Becke, A. D. *J. Chem. Phys.* **1993**, *98*, 5648–5652.
- (51) Stephens, P. J.; Devlin, F. J.; Chabalowski, C. F.; Frisch, M. J. *J. Phys. Chem.* **1994**, *98*, 11623–11627.
- (52) Lee, C. T.; Yang, W. T.; Parr, R. G. *Phys. Rev. B* **1988**, *37*, 785–789.
- (53) Henkelman, G.; Uberuaga, B. P.; Jonsson, H. *J. Chem. Phys.* **2000**, *113*, 9901–9904.
- (54) Kästner, J.; Carr, J. M.; Keal, T. W.; Thiel, W.; Wander, A.; Sherwood, P. *J. Phys. Chem. A* **2009**, *113*, 11856–11865.
- (55) Frisch, M. J.; et al. *Gaussian 03*, revision D.01; Gaussian Inc.: Wallingford, CT, 2004.
- (56) Humphrey, W.; Dalke, A.; Schulten, K. *J. Mol. Graphics* **1996**, *14*, 33–38.
- (57) Hay, P. J.; Wadt, W. R. *J. Chem. Phys.* **1985**, *82*, 270–283.
- (58) Ehlers, A. W.; Böhme, M.; Dapprich, S.; Gobbi, A.; Höllwarth, A.; Jonas, V.; Köhler, K. F.; Stegmann, R.; Veldkamp, A.; Frenking, G. *Chem. Phys. Lett.* **1993**, *208*, 111–114.
- (59) Wadt, W. R.; Hay, P. J. *J. Chem. Phys.* **1985**, *82*, 284–298.
- (60) Höllwarth, A.; Böhme, M.; Dapprich, S.; Ehlers, A. W.; Gobbi, A.; Jonas, V.; Köhler, K. F.; Stegmann, R.; Veldkamp, A.; Frenking, G. *Chem. Phys. Lett.* **1993**, *208*, 237–240.
- (61) Hariharan, P. C.; Pople, J. A. *Theor. Chim. Acta* **1973**, *28*, 213–222.
- (62) Clark, T.; Chandrasekhar, J.; Spitznagel, G. W.; Schleyer, P. v. R. *J. Comput. Chem.* **1983**, *4*, 294–301.
- (63) Weigend, F. *Phys. Chem. Chem. Phys.* **2006**, *8*, 1057–1065.
- (64) Kim, J. H.; Odutola, J. A.; Popham, J.; Jones, L.; von Laven, S. *J. Inorg. Biochem.* **2001**, *84*, 145–150.
- (65) Eyring, H. *J. Chem. Phys.* **1935**, *3*, 107–115.
- (66) Sevastik, R.; Himo, F. *Bioorg. Chem.* **2007**, *35*, 444–457.
- (67) Hopmann, K. H.; Himo, F. *J. Chem. Theory Comput.* **2008**, *4*, 1129–1137.
- (68) Chen, S.-L.; Fang, W.-H.; Himo, F. *Theor. Chem. Acc.* **2008**, *120*, 515–522.
- (69) Siegbahn, P. E. M.; Himo, F. *J. Biol. Inorg. Chem.* **2009**, *14*, 643–651.

JP909999S